HHS Public Access

Author manuscript

*Radiother Oncol*. Author manuscript; available in PMC 2015 December 02.

Published in final edited form as:

*Radiother Oncol*. 2013 October ; 109(1): 65–70. doi:10.1016/j.radonc.2013.08.032.

# Characterization of tumour heterogeneity using dynamic contrast enhanced CT and FDG-PET in non-small cell lung cancer

**W. van Elmpt**[1], **M. Das**[2], **Martin Hüllner**[3,**], **H. Sharifi**[1], **K. Zegers**[1], **B. Reymen**[1], **P. Lambin**[1], **J.E. Wildberger**[2], **E.G.C. Troost**[1], **P. Veit-Haibach**[#3,**], and **D. De Ruysscher**[#1,4]

[1]Department of Radiation Oncology (MAASTRO), GROW – School for Oncology and Developmental Biology, Maastricht University Medical Centre, Maastricht, The Netherlands [2]Department of Radiology, GROW – School for Oncology and Developmental Biology, Maastricht University Medical Centre, Maastricht, The Netherlands [3]Department of Radiology, Cantonal Hospital Lucerne, Lucerne, Switzerland [4]Radiation Oncology, University Hospitals Leuven/ KU Leuven, Leuven, Belgium

[#] These authors contributed equally to this work.

## Abstract

**Purpose—**Dynamic contrast-enhanced CT (DCE-CT) quantifies vasculature properties of tumours, whereas static FDG-PET/CT defines metabolic activity. Both imaging modalities are capable of showing intra-tumour heterogeneity. We investigated differences in vasculature properties within primary non-small cell lung cancer (NSCLC) tumours measured by DCE-CT and metabolic activity from FDG-PET/CT.

**Methods—**33 NSCLC patients were analysed prior to treatment. FDG-PET/CT and DCE-CT were co-registered. The tumour was delineated and metabolic activity was segmented on the FDG-PET/CT in two regions: low (<50% maximum SUV) and high (≥50% maximum SUV) metabolic uptake. Blood flow, blood volume and permeability were calculated using a maximum slope, deconvolution algorithm and a Patlak model. Correlations were assessed between perfusion parameters for the regions of interest.

**Results—**DCE-CT provided additional information on vasculature and tumour heterogeneity that was not correlated to metabolic tumour activity. There was no significant difference between low and high metabolic active regions for any of the DCE-CT parameters. Furthermore, only moderate correlations between maximum SUV and DCE-CT parameters were observed.

*Corresponding author:* Wouter van Elmpt, Ph.D., Department of Radiation Oncology (MAASTRO), GROW – School for Oncology and Developmental Biology, Maastricht University Medical Centre, Dr. Tanslaan 12, NL-6229 ET Maastricht, The Netherlands, Tel.: +31 88 44 55 666, Fax.: +31 88 44 55 667, wouter.vanelmpt@maastro.nl.

[**]Present address: University Hospital Zurich, Department of Medical Imaging, 8091 Zurich, Switzerland.

*Conflict of interest*: J.E. Wildberger received grants and travel support from Siemens R&D.

**Conclusion—**No direct correlation was observed between FDG-uptake and parameters extracted from DCE-CT. DCE-CT may provide complementary information to the characterization of primary NSCLC tumours over FDG-PET/CT imaging.

### Keywords

dynamic contrast enhanced (DCE) CT; perfusion CT imaging; FDG-PET; NSCLC; image analysis

## Introduction

One of the hallmarks of cancer is angiogenesis [1]. As a result of the abundant and non-structured production of angiogenic proteins, blood vessels in tumours become abnormal. Paradoxically, tumour angiogenesis therefore leads to hypoxia, one of the most important triggers for tumour progression, metastasis formation and treatment resistance [2]. As angiogenesis can indirectly be quantified by perfusion, techniques to determine blood flow have gained increasing interest. $^{18}$F-deoxyglucose (FDG) uptake by means of PET scans is used to stage non-small cell lung cancer (NSCLC) and has prognostic value as well [3,4]. FDG uptake is related to many biological processes, including glucose metabolism and hypoxia [5]. Angiogenesis and FDG uptake thus define distinct, though relevant biological processes.

With the introduction of the latest state-of-the-art CT scanners, volumetric imaging using dynamic contrast-enhanced CT imaging (DCE-CT) of primary lung cancer is now possible [6-8]. Parameters derived from DCE-CT in NSCLC were previously shown to correlate with tumour characteristics such as micro vessel density (MVD) [9-11] and negative correlations between blood vessel permeability and the glucose transporter (Glut-1) receptor [12] were observed. Li *et al* demonstrated a direct strong correlation between blood volume and MVD in a heterogeneous group of peripheral lung cancers, proposing DCE-CT for the *in-vivo* evaluation of necrosis and neoangiogenesis [11].

Furthermore, DCE-CT was found to correlate with the gold standard of perfusion, [(15)O]H2O-PET [13]. Although dynamic FDG acquisitions may also give insight of tumour perfusion, in routine clinical practice, static PET scans are used. Static high FDG-uptake patterns prior to treatment have been shown to identify resistance areas within a tumour indicated by residual metabolic tumour activity in follow-up imaging after radiotherapy [14-16]. It is therefore of interest to investigate the correlations between vasculature parameters derived from DCE-CT and metabolic imaging parameters from FDG-PET/CT [17]. However, previous studies found mixed results, i.e. some studies showing positive [18], others inverse [19,20] or no correlation [20-22] between FDG-PET and DCE-CT parameters. Furthermore, typically these studies report only modest correlation coefficients around 0.5. This suggests possible complementary information of DCE-CT compared to FDG-PET imaging, the first one being more specific for quantification of vasculature properties and the second identifying metabolic status of the tumour. Quantification of tumour heterogeneity by combining vasculature and metabolic properties of the tumour could in future be important factors to use for treatment individualization [23-25].

In the context of radiotherapy of non-small cell lung cancer, few DCE-CT imaging studies are being performed. Permeability derived from DCE-CT was hypothesized to relate to tumour response or outcome after (chemo-)radiotherapy [21,26]. During radiotherapy, different spatial uptake patterns between the core and the rim of the tumour were described, with the latter being more vascularized [27]. However, the authors did not investigate and compare the results with the FDG-uptake pattern.

The aim of this study was two-fold, first to investigate the heterogeneity of vasculature within primary NSCLC for various frequently used kinetic algorithms and secondly to compare the extracted perfusion parameters from DCE-CT with different metabolically active regions defined on FDG-PET.

## Materials and Methods

### Patient characteristics

We analysed advanced stage NSCLC patients (stage II & III) from two different hospitals. Images were acquired at the Maastricht University Medical Centre (MUMC, Maastricht, The Netherlands) (dataset A, NCT01024829 and NCT01210378) and the Cantonal Hospital Luzern (Switzerland) (dataset B, Cantonal Ethics Trial Nr.1000) prior to intended (chemo-) radiotherapy treatment.

### DCE-CT image acquisition

DCE-CT imaging was performed on a second generation dual source CT scanner (Definition Flash; Siemens Healthcare, Forchheim, Germany) in both centres. Image acquisition was performed using either 80 kVp/120 mAs (dataset A) or 100 kVp/100 mAs setting (dataset B). Using a cranial caudal field of view of 13 cm (dataset A) and 7 cm (dataset B) centred on the primary tumour at a slice thickness of 5 mm. The first 50 sec (dataset A) or 60 sec (dataset B) were scanned at a cycle time of 1.5 s and 1.0 s per image, for dataset A and B, respectively, and captured with a delay of two (dataset A) or three (dataset B) seconds after start of the contrast injection. The contrast agent was iodine based, either using 60 ml iopromide (Ultravist 300, Bayer Healthcare, Berlin, Germany) injected at 7.0 ml/s for dataset A or 40 ml (Ultravist 370) injected at 4.5 ml/s for dataset B. Patients were advised to do a breath-hold at expiration or resume shallow breathing for the entire duration of the scan. Image reconstruction encompassing the entire thorax was performed with a 512 × 512 pixel matrix and (medium) smooth B20f (dataset A) or B30f (dataset B) kernel.

### FDG-PET/CT acquisition

On the same day of the DCE-CT, patients underwent an FDG-PET/CT acquisition on an integrated PET/CT scanner according to institutional protocols. Image acquisition started 1 hour after injection of approximately 250 MBq FDG (depending on patient weight) on a Siemens Biograph 40 PET/CT (Siemens Healthcare, Erlangen, Germany) for dataset A or on a GE Discovery 600 PET/CT scanner (GE Healthcare, Waekesha (WI), USA) for dataset B. Images were converted into standardized uptake values (SUV) correcting for injected activity and body weight.

### DCE-CT and SUV analysis

Tumour volumes of the primary tumour were manually delineated on the PET/CT scan by experienced radiation oncologists. Tumour volumes were also classified as small or large tumours using a cut-off of 30 $cm^3$ [19]. Metabolic uptake regions within this primary tumour were automatically segmented using the FDG-PET images and divided into a low (0-50% of the maximum SUV) and high metabolic uptake (≥50% of the maximum SUV). The 50% SUVmax cut-off has been hypothesized to contain residual disease after treatment [15] and is used as target in on-going dose-boosting trials [28]. Additionally, the maximum SUV inside the region of interest was extracted. Furthermore, an analysis according to histological subtype was performed.

Subsequently, the CT scan of the PET/CT acquisition and the first frame (time point) of the DCE-CT scan were non-rigidly registered using previous validated in-house developed software [29]. The contours of the primary tumour, low and high uptake regions on the PET/CT scan were copied to the DCE-CT. In order to assure correct calculation, the deformation fields were visually assessed. By transferring the contour of the region of interest from one image set to the other, we prevent interpolation issues from down and up scaling that might distort the original image (e.g. SUV) values that could occur if the images itself are deformed. Parameters from the DCE-CT were calculated using commercial software (Siemens VPCT body (VE36A), Siemens Healthcare, Forchheim, Germany). Both motion correction and noise reduction algorithms implemented in the software were applied. For the arterial input function a region of interest was chosen inside the aortic arch. Three kinetic analysis algorithms were calculated: maximum slope model (S), a deconvolution algorithm (A) and a Patlak (P) analysis. From these algorithms various parameters for the primary tumour were extracted. Blood flow (BF) was extracted for the maximum slope and deconvolution algorithm, blood volume (BV) for all three algorithms, and a measure of permeability (PMB) was calculated for the deconvolution and Patlak model. For the primary tumour, low and high uptake regions, the average blood flow, blood volume and permeability were calculated. Voxel-by-voxel parameter maps were exported and combined with the volume of interest defined on the PET/CT images. Average blood flow, volume and permeability parameters were then calculated for the specific parameter under investigation. Also, correlations between the extracted parameters within the algorithms and between different kinetic models were assessed.

### Statistics

Differences between two groups were compared using a Student's t-test or a one-way ANOVA testing for multiple groups, whereas paired statistics were calculated using the paired t-test. Correlations were assessed using linear regression and Pearson's coefficient $r$ with $r<0.3$ indicating small or no correlation, $0.3<r<0.5$ for moderate and $r>0.5$ for strong correlations. Values of $p < 0.05$ were considered as statistically significant.

## Results

In total 33 patients were included in the analysis, 11 patients from dataset A and 22 patients from dataset B. There were no significant differences between dataset A and B in

distribution of the maximum SUV (p=0.45) or extracted perfusion parameters (range p-values: 0.15 to 0.86), therefore we pooled both datasets for subsequent analysis. An example of a patient is shown in Figure 1.

Two types of correlations were assessed for the parameters extracted within the primary tumour. First, correlation between the average extracted parameters between different models was assessed. Blood flow correlated strongly between the maximum slope and deconvolution model, r=0.91 (p<0.001), however, the slope between both models was 2.08 indicating an almost double parameter estimation for the deconvolution model compared to the maximum slope model. For blood volume, correlations were also strong: maximum slope *versus* deconvolution algorithm: r=0.94 (p=0.001, slope: 1.01); maximum slope *versus* Patlak: r=0.70 (p<0.001, slope: 0.76); and deconvolution algorithm *versus* Patlak: r=0.72 (p<0.001, slope: 0.74). For permeability the correlation parameters were r=0.68 (p<0.001), slope: 0.69 between the deconvolution and Patlak model.

Second, we investigated the correlation between the various perfusion parameters within one algorithm; see Supplemental Figure S1 for the results of the deconvolution algorithm. For the maximum slope algorithm (2 kinetic parameters extracted), blood flow was highly correlated with blood volume (r=0.91, p<0.001). For the deconvolution algorithm (3 parameters estimated), blood flow and blood volume were also highly correlated (r=0.77, p<0.001) as well as permeability and blood volume (r=0.71, p<0.001), and to a lesser extent also blood flow and permeability (r=0.59, p<0.001; Supplemental Figure S1). For the Patlak model (2 parameters estimated) blood volume and permeability were not correlated (r=0.26, p=0.15).

There was no statistical difference between perfusion parameters extracted for small or large tumours (p>0.2 for all parameters; Table 1). Maximum SUV showed a difference between small and large tumours: 4.5 ± 2.3 (1SD) and 6.5 ± 2.8 (p=0.008), respectively.

In Figure 2, the (non-) correlation between maximum SUV and perfusion parameters derived for the deconvolution algorithm are shown. These correlations were non-significant for PMB (p=0.13) and only moderate correlated for BF (r=0.45, p=0.008) and BV (r=0.35, p=0.04). Similar results, were found for the maximum slope method (BF: r=0.35, p=0.04, BV: r=0.41, p=0.02) and Patlak model (BV: p=0.07, PMB: r=0.41, p=0.02) showing moderate correlation with the maximum FDG-uptake.

There was no significant difference between the high and low-uptake FDG regions (Figure 3 and Table 2). Although permeability extracted using the deconvolution algorithm showed higher values for the high metabolic uptake region, this did not reach significance (p=0.08).

Also for histological subtypes, grouped between adenocarcinoma (N=15), squamous cell carcinoma (N=8), large cell carcinoma (N=9) and one neuroendocrine tumour, results did not show statistical differences, see Supplemental Table S1.

## Discussion

DCE-CT is a suitable technique for visualization and quantification of heterogeneity in vasculature of NSCLC tumours. Blood flow and volume are both indirect measures of tumour angiogenesis, which has shown to be measurable with perfusion studies [30,31]. Perfusion parameters extracted using the frequently used kinetic models in DCE-CT did not show strong correlations with static FDG-uptake in primary non-small cell lung cancer tumours indicating additional quantitative characteristics of the primary tumour. Perfusion parameters within the high and low metabolically active regions did not show large differences which may suggest that there is no difference in vasculature between metabolically active and non-active regions. DCE-CT thus gives additional information on vasculature that is not directly related to metabolic tumour activity. Some authors already suggested such a decoupling between perfusion characteristics and metabolic activity for larger tumour volumes [19,20]. This is in line with our dataset where even though the majority of primary tumours were fairly large in size, we did not observe a correlation between any of the perfusion parameters and metabolic activity. Furthermore, this study shows that besides for tumour size this decoupling might also hold true within the primary tumour, where no differences were found between metabolic (non-) active regions.

There was a high correlation between similar extracted parameters on DCE-CT that were calculated using different models, *e.g.* the blood flow extracted using the maximum slope model and the deconvolution algorithm had a strong correlation. Furthermore, it is worthwhile to note that the deconvolution algorithm had typically a twice as high value for blood flow. Smaller discrepancies between the various algorithms were found for blood volume and permeability. This discrepancy has previously been shown for other software packages and models [32].

There are several restrictions and limitations that have to be taken into account for the interpretation of DCE-CT studies. First, for this study we used data from two centres having slightly different acquisition procedures (e.g., acquisition length, iodine delivery rates and temporal resolution). However, for the current study we could not identify a difference in extracted parameters for both centres. Furthermore, fast CT acquisition techniques can be performed in breath hold or provide a snapshot of the tumour during the breathing cycle. Compared to a PET technique one has to realize that PET imaging is typically performed using a 3D acquisition over multiple breathing cycles causing blurring due to breathing motion and possible patient movement. Hence, registration between (DCE-)CT and PET/CT images has to be evaluated carefully especially in transferring regions of interest from one dataset to the other.

Second, to assess permeability of vasculature typically longer acquisition times of up to 3 or 5 minutes have been used, whereas our perfusion protocols were (first-pass) perfusion of the tumour during the first minute after contrast administration. Extending acquisition time may give better estimations of the permeability and thus future studies need to be explored whether estimation of the permeability using longer acquisition durations is correlated with metabolic uptake [30].

Third, validation of kinetic analysis software is not trivial. The commercial software package we used in this study has been used by others to compare functional imaging parameters against histology [10]. However, in general, most commercial software solutions are black-box systems with build-in smoothing, noise reduction and automatic fitting procedures that are not directly interchangeable [32]. Thorough validation and benchmarking against other kinetic analysis models, e.g. an extended Tofts model or approximated adiabatic expansion model are necessary. Selecting a sound kinetic analysis model is topic of investigation for various groups and may need to be tailored to different tumour sites [33,34].

Lastly, in contradiction to some but not all literature [18,19], we did not find strong correlations between FDG-uptake measured on PET imaging and perfusion characteristics in non-small cell lung cancer. Several authors describe significant correlations, however, in our study these correlations appear to be weak or at maximum modest with moderate correlation coefficients, we therefore cannot conclude that metabolic and vasculature properties are linked using the current imaging and analysis methodology. Hence FDG uptake and perfusion derived parameters show distinct biological characteristics allowing further characterizing tumour heterogeneity that should be investigated in future as an independent factor for treatment outcome.

With the current frequently used first-pass perfusion protocols no correlation between metabolic uptake visualized on FDG-PET/CT imaging and extracted DCE-CT parameters was found. Further research in optimizing the acquisition settings and kinetic analysis models are necessary for exploration of the added value of DCE-CT for NSCLC.

## Supplementary Material

Refer to Web version on PubMed Central for supplementary material.

## Acknowledgement

We acknowledge financial support from the CTMM framework (AIRFORCE project), EU 6th and 7th framework program (ARTFORCE and METOXIA program), Interreg (www.eurocat.info), STW (DuCAT), the Kankeronderzoekfonds Limburg from the Health Foundation Limburg and the Dutch Cancer Society (KWF UM 2011-5020). One of the authors (W.v.E.) would like to acknowledge funding (KWF MAC 2011-4970) from the Dutch Cancer Society. The study data acquisition in Lucerne was partially supported by Bayer Healthcare. Patrick Veit-Haibach received an ISS Grant from Bayer Healthcare for PET/CT with integrated CT-perfusion in bronchial carcinoma.

## References

1. Carmeliet P, Jain RK. Molecular mechanisms and clinical applications of angiogenesis. Nature. 2011; 473:298–307. [PubMed: 21593862]
2. Wilson WR Hay MP. Targeting hypoxia in cancer therapy. Nat Rev Cancer. 2011; 11:393–410. [PubMed: 21606941]
3. De Ruysscher D, Kirsch CM. PET scans in radiotherapy planning of lung cancer. Radiother Oncol. 2010; 96:335–338. [PubMed: 20656364]
4. MacManus M, Nestle U, Rosenzweig KE, et al. Use of PET and PET/CT for radiation therapy planning: IAEA expert report 2006-2007. Radiother Oncol. 2009; 91:85–94. [PubMed: 19100641]

5. van Baardwijk A, Dooms C, van Suylen RJ, et al. The maximum uptake of (18)F-deoxyglucose on positron emission tomography scan correlates with survival, hypoxia inducible factor-1alpha and GLUT-1 in non-small cell lung cancer. Eur J Cancer. 2007; 43:1392–1398. [PubMed: 17512190]
6. Goh V, Ng QS Miles K. Computed tomography perfusion imaging for therapeutic assessment: has it come of age as a biomarker in oncology? Invest Radiol. 2012; 47:2–4. [PubMed: 21808202]
7. Garcia-Figueiras R, Goh VJ, Padhani AR, et al. CT perfusion in oncologic imaging: a useful tool? AJR Am J Roentgenol. 2013; 200:8–19. [PubMed: 23255736]
8. Ng CS, Chandler AG, Wei W, et al. Reproducibility of perfusion parameters obtained from perfusion CT in lung tumors. AJR Am J Roentgenol. 2011; 197:113–121. [PubMed: 21701018]
9. Tacelli N, Remy-Jardin M, Copin MC, et al. Assessment of non-small cell lung cancer perfusion: pathologic-CT correlation in 15 patients. Radiology. 2010; 257:863–871. [PubMed: 20843993]
10. Sauter AW, Winterstein S, Spira D, et al. Multifunctional profiling of non-small cell lung cancer using 18F-FDG PET/CT and volume perfusion CT. J Nucl Med. 2012; 53:521–529. [PubMed: 22414637]
11. Li Y, Yang ZG, Chen TW, Chen HJ, Sun JY Lu YR. Peripheral lung carcinoma: correlation of angiogenesis and first-pass perfusion parameters of 64-detector row CT. Lung Cancer. 2008; 61:44–53. [PubMed: 18055062]
12. Mandeville HC, Ng QS, Daley FM, et al. Operable non-small cell lung cancer: correlation of volumetric helical dynamic contrast-enhanced CT parameters with immunohistochemical markers of tumor hypoxia. Radiology. 2012; 264:581–589. [PubMed: 22700554]
13. Kramer GM, Yaqub M, Bahce I, et al. CT-perfusion versus [(15)O]H2O PET in lung tumors: Effects of CT-perfusion methodology. Med Phys. 2013; 40:052502. [PubMed: 23635292]
14. Abramyuk A, Tokalov S, Zophel K, et al. Is pre-therapeutical FDG-PET/CT capable to detect high risk tumor subvolumes responsible for local failure in non-small cell lung cancer? Radiother Oncol. 2009; 91:399–404. [PubMed: 19168248]
15. Aerts HJ, van Baardwijk AA, Petit SF, et al. Identification of residual metabolic-active areas within individual NSCLC tumours using a pre-radiotherapy (18)Fluorodeoxyglucose-PET-CT scan. Radiother Oncol. 2009; 91:386–392. [PubMed: 19329207]
16. Petit SF, Aerts HJ, van Loon JG, et al. Metabolic control probability in tumour subvolumes or how to guide tumour dose redistribution in non-small cell lung cancer (NSCLC): an exploratory clinical study. Radiother Oncol. 2009; 91:393–398. [PubMed: 19328570]
17. Hansen AE, Kristensen AT, Law I, McEvoy FJ, Kjaer A Engelholm SA. Multimodality functional imaging of spontaneous canine tumors using 64Cu-ATSM and 18FDG PET/CT and dynamic contrast enhanced perfusion CT. Radiother Oncol. 2012; 102:424–428. [PubMed: 22119225]
18. Ohno Y, Koyama H, Matsumoto K, et al. Differentiation of malignant and benign pulmonary nodules with quantitative first-pass 320-detector row perfusion CT versus FDG PET/CT. Radiology. 2011; 258:599–609. [PubMed: 21273522]
19. Ippolito D, Capraro C, Guerra L, De Ponti E, Messa C Sironi S. Feasibility of perfusion CT technique integrated into conventional 18FDG/PET-CT studies in lung cancer patients: clinical staging and functional information in a single study. Eur J Nucl Med Mol Imaging. 2013; 40:156–165. [PubMed: 23143661]
20. Sauter AW, Spira D, Schulze M, et al. Correlation between [(18)F]FDG PET/CT and volume perfusion CT in primary tumours and mediastinal lymph nodes of non-small-cell lung cancer. Eur J Nucl Med Mol Imaging. 2013; 40:677–684. [PubMed: 23306806]
21. Lazanyi KS, Abramyuk A, Wolf G, et al. Usefulness of dynamic contrast enhanced computed tomography in patients with non-small-cell lung cancer scheduled for radiation therapy. Lung Cancer. 2010; 70:280–285. [PubMed: 20371133]
22. Miles KA, Griffiths MR Keith CJ. Blood flow-metabolic relationships are dependent on tumour size in non-small cell lung cancer: a study using quantitative contrast-enhanced computer tomography and positron emission tomography. Eur J Nucl Med Mol Imaging. 2006; 33:22–28. [PubMed: 16180030]
23. Lambin P, Petit SF, Aerts HJ, et al. The ESTRO Breur Lecture 2009. From population to voxel-based radiotherapy: exploiting intra-tumour and intra-organ heterogeneity for advanced treatment of non-small cell lung cancer. Radiother Oncol. 2010; 96:145–152. [PubMed: 20647155]

24. Lambin P, van Stiphout RG, Starmans MH, et al. Predicting outcomes in radiation oncology--multifactorial decision support systems. Nat Rev Clin Oncol. 2013; 10:27–40. [PubMed: 23165123]

25. Hermans R, Lambin P, Van der Goten A, et al. Tumoural perfusion as measured by dynamic computed tomography in head and neck carcinoma. Radiother Oncol. 1999; 53:105–111. [PubMed: 10665786]

26. Wang J, Wu N, Cham MD Song Y. Tumor response in patients with advanced non-small cell lung cancer: perfusion CT evaluation of chemotherapy and radiation therapy. AJR Am J Roentgenol. 2009; 193:1090–1096. [PubMed: 19770333]

27. Ng QS, Goh V, Milner J, Padhani AR, Saunders MI Hoskin PJ. Acute tumor vascular effects following fractionated radiotherapy in human lung cancer: In vivo whole tumor assessment using volumetric perfusion computed tomography. Int J Radiat Oncol Biol Phys. 2007; 67:417–424. [PubMed: 17236965]

28. van Elmpt W, De Ruysscher D, van der Salm A, et al. The PET-boost randomised phase II dose-escalation trial in non-small cell lung cancer. Radiother Oncol. 2012; 104:67–71. [PubMed: 22483675]

29. Orban de Xivry J, Janssens G, Bosmans G, et al. Tumour delineation and cumulative dose computation in radiotherapy based on deformable registration of respiratory correlated CT images of lung cancer patients. Radiother Oncol. 2007; 85:232–238. [PubMed: 17936388]

30. de Langen AJ, van den Boogaart V, Lubberink M, et al. Monitoring response to antiangiogenic therapy in non-small cell lung cancer using imaging markers derived from PET and dynamic contrast-enhanced MRI. J Nucl Med. 2011; 52:48–55. [PubMed: 21149474]

31. Ren Y, Fleischmann D, Foygel K, et al. Antiangiogenic and radiation therapy: early effects on in vivo computed tomography perfusion parameters in human colon cancer xenografts in mice. Invest Radiol. 2012; 47:25–32. [PubMed: 22178893]

32. Goh V, Shastry M, Engledow A, et al. Commercial software upgrades may significantly alter Perfusion CT parameter values in colorectal cancer. Eur Radiol. 2011; 21:744–749. [PubMed: 20922392]

33. Koh TS, Ng QS, Thng CH, Kwek JW, Kozarski R Goh V. Primary colorectal cancer: use of kinetic modeling of dynamic contrast-enhanced CT data to predict clinical outcome. Radiology. 2013; 267:145–154. [PubMed: 23297334]

34. Korporaal JG, van Vulpen M, van den Berg CA, van der Heide UA. Tracer kinetic model selection for dynamic contrast-enhanced computed tomography imaging of prostate cancer. Invest Radiol. 2012; 47:41–48. [PubMed: 21610505]

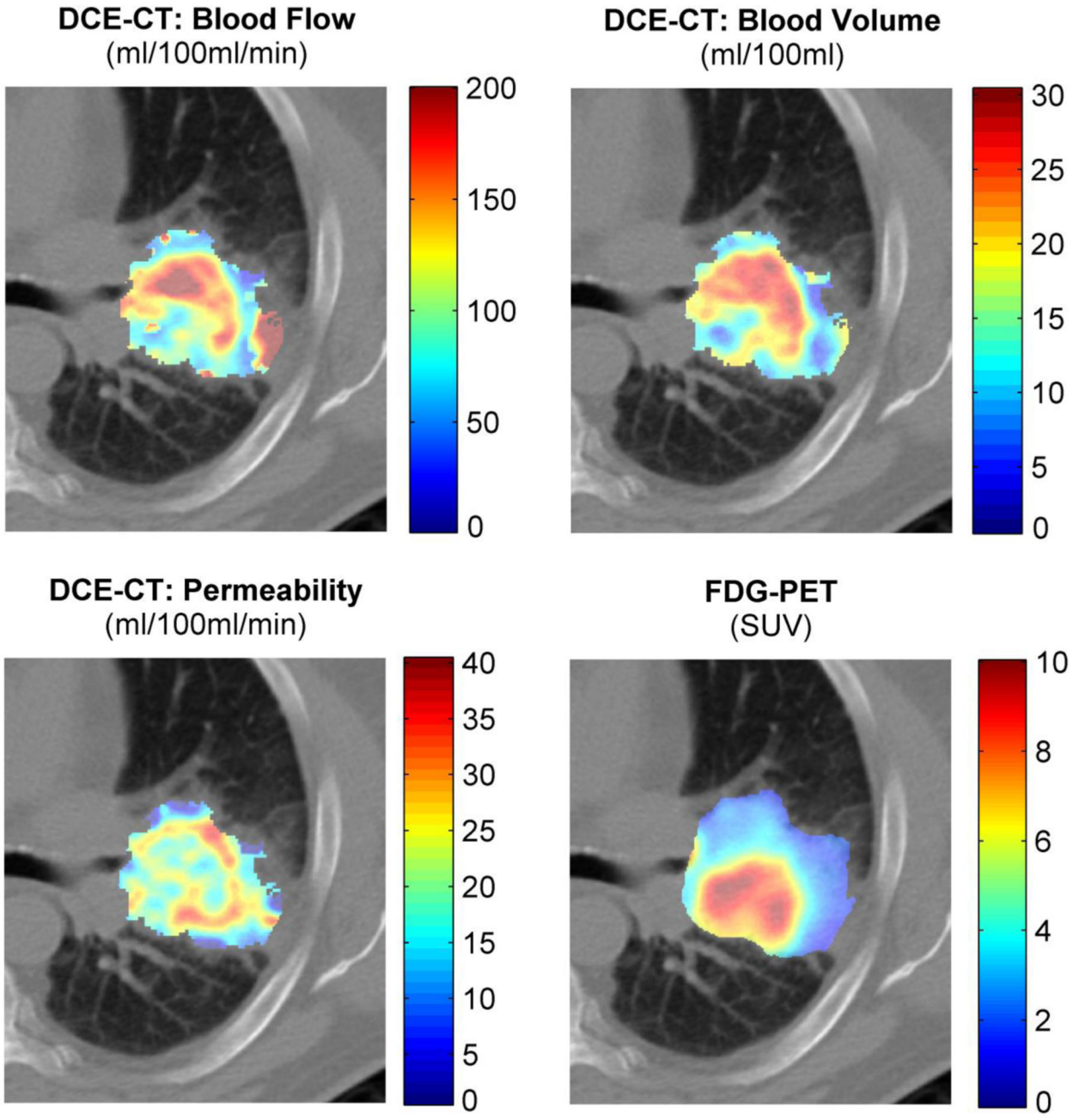


**Figure 1.**
DCE-CT and FDG-PET example of a patient.

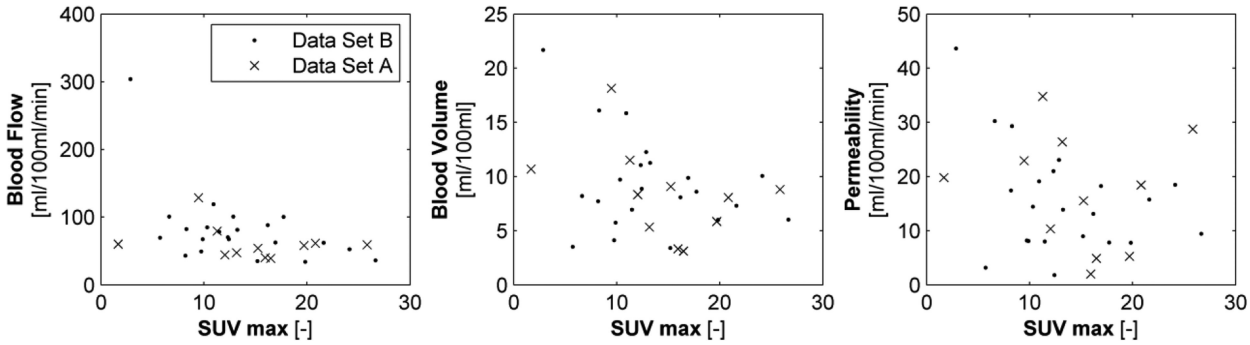


**Figure 2.**

Scatter plot of the extracted kinetic parameters (blood flow (left), blood volume (middle) and permeability (right panel) calculated using the deconvolution algorithm and maximum SUV inside the primary lung tumour.

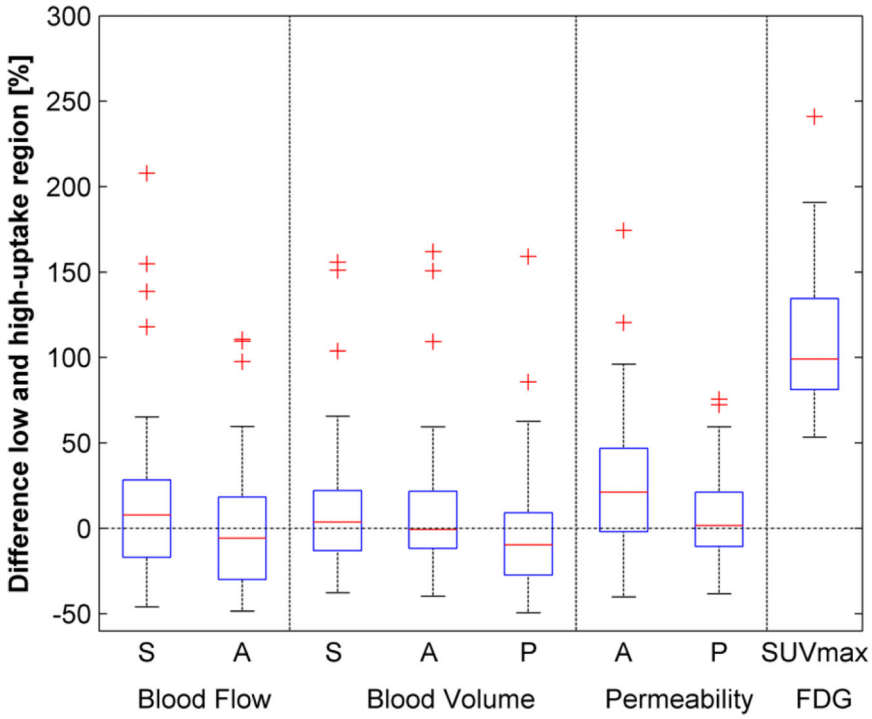


**Figure 3.**

Box-plot of the differences between the calculated perfusion parameters for the low and high uptake regions inside the primary tumour for the maximum slope (S), deconvolution algorithm (A) and Patlak model (P). Only maximum SUV showed a significant increase of 108% between both regions ($p<0.001$) due to the definition of the two regions of interest.

**Table 1**

Overview of the extracted perfusion parameters for the entire primary tumour, small and large tumours. P-values are calculated using a t-test between small and large tumours.

| | | All tumours (N=33) | Small tumours (<30cm$^3$) (N=8) | Large tumours (>30 cm$^3$) (N=25) | small *versus* large tumours |
|---|---|---|---|---|---|
| | | mean ± SD | mean ± SD | mean ± SD | p-value |
| **Blood Flow** *[ml/100ml/min]* | **Maximum slope** | 36.5 ± 20.8 | 39.2 ± 34.6 | 35.7 ± 14.9 | 0.996 |
| | **Deconvolution alg.** | 74.7 ± 47.7 | 92.7 ± 87.0 | 68.9 ± 26.1 | 0.250 |
| **Blood Volume** *[ml/100ml]* | **Maximum slope** | 7.4 ± 4.0 | 9.1 ± 6.4 | 6.9 ± 2.9 | 0.374 |
| | **Deconvolution alg.** | 8.9 ± 4.3 | 10.7 ± 5.9 | 8.4 ± 3.6 | 0.434 |
| | **Patlak** | 7.9 ± 4.4 | 8.3 ± 4.8 | 7.8 ± 4.4 | 0.969 |
| **Permeability** *[ml/100ml/min]* | **Deconvolution alg.** | 16.1 ± 10.0 | 17.9 ± 13.4 | 15.5 ± 8.9 | 0.885 |
| | **Patlak** | 21.6 ± 9.7 | 26.4 ± 9.8 | 20.0 ± 9.3 | 0.222 |
| **FDG-PET** *[SUV]* | **Mean SUV** | 6.1 ± 2.8 | 4.5 ± 2.3 | 6.5 ± 2.8 | <0.001 |
| | **Maximum SUV** | 13.8 ± 6.1 | 9.0 ± 4.8 | 15.3 ± 5.7 | 0.008 |

N, number; SD, standard deviation; alg, algorithm; SUV, standardized uptake value.

**Table 2**

Overview of the extracted perfusion parameters for the low and high uptake regions inside the primary tumour. P-values are calculated using a paired t-test between low and high FDG-uptake values.

| | | Low FDG-uptake region (<50% maximum SUV) | High FDG-uptake region (>50% maximum SUV) | low *versus* high uptake |
|---|---|---|---|---|
| | | mean ± SD | mean ± SD | p-value |
| **Blood Flow** *[ml/100ml/min]* | **Maximum slope** | 39.0 ± 32.3 | 39.2 ± 20.8 | 0.961 |
| | **Deconvolution alg.** | 83.0 ± 62.1 | 74.6 ± 46.6 | 0.117 |
| **Blood Volume** *[ml/100ml]* | **Maximum slope** | 7.8 ± 5.7 | 8.0 ± 4.0 | 0.732 |
| | **Deconvolution alg.** | 9.2 ± 5.5 | 9.6 ± 4.3 | 0.472 |
| | **Patlak** | 8.6 ± 4.6 | 8.2 ± 5.1 | 0.547 |
| **Permeability** *[ml/100ml/min]* | **Deconvolution alg.** | 15.7 ± 12.9 | 18.6 ± 13.0 | 0.080 |
| | **Patlak** | 21.4 ± 9.6 | 22.5 ± 10.2 | 0.181 |
| **FDG-PET** *[SUV]* | **Mean SUV** | 4.3 ± 1.8 | 9.0 ± 3.9 | <0.001 |
| | **Maximum SUV** | 7.6 ± 3.7 | 13.8 ± 6.1 | <0.001 |

SD, standard deviation; alg, algorithm; SUV, standardized uptake value.